LLNL'S PRECISION COMPTON SCATTERING LIGHT SOURCE*

F.V. Hartemann#, F. Albert, S. G. Anderson, A.J. Bayramian, R.R. Cross, C.A. Ebbers, D. J. Gibson, T.L. Houck, R.A. Marsh, M. J. Messerly, V. A. Semenov, M.Y. Shverdin, S.S. Wu, R.D. Scarpetti, Jr., C.W. Siders, D.P. McNabb, R.E. Bonanno, and C.P.J. Barty, LLNL, Livermore, CA 94550, U.S.A.
C.E. Adolphsen, A. Candel, T.S. Chu, E.N. Jongewaard, Z. Li, C. Limborg-Deprey, S.G. Tantawi, A.E. Vlieks, F. Wang, J.W. Wang, F. Zhou, and T.O. Raubenheimer, SLAC, Stanford, CA 94025, U.S.A.

Abstract

Continued progress in accelerator physics and laser technology have enabled the development of a new class of tunable x-ray and gamma-ray light sources based on Compton scattering between a high-brightness, relativistic electron beam and a high intensity laser pulse produced via chirped-pulse amplification (CPA). A precision, tunable, monochromatic (< 0.4% *rms* spectral width) source driven by a compact, high-gradient X-band linac designed in collaboration with SLAC is under construction at LLNL. High-brightness (250 pC, 2 ps, 0.4 mm.mrad), relativistic electron bunches will interact with a Joule-class, 10 ps, diode-pumped CPA laser pulse to generate tunable γ-rays in the 0.5-2.5 MeV photon energy range. This gamma-ray source will be used to excite nuclear resonance fluorescence in various isotopes. Fields of endeavor include homeland security, stockpile science and surveillance, nuclear fuel assay, and waste imaging and assay. The source design, key parameters, and current status will be discussed, along with important applications, including nuclear resonance fluorescence and high precision medical imaging.

INTRODUCTION AND OVERVIEW

The nascent field of nuclear photonics is enabled by the recent maturation of new technologies, including high-gradient X-band electron acceleration, robust fiber laser systems, and hyper-dispersion CPA [1]. Recent work has been performed at LLNL to demonstrate isotope-specific detection of shielded materials via NRF using a tunable, quasi-monochromatic Compton scattering gamma-ray source operating between 0.2 MeV and 0.9 MeV photon energy. This technique is called Fluorescence Imaging in the Nuclear Domain with Energetic Radiation (or FINDER). This work has, among other things, demonstrated the detection of ^{7}Li shielded by Pb, utilizing gamma rays generated by a linac-driven, laser-based Compton scattering gamma-ray source developed at LLNL [2-4]. Within this context, a new facility is currently under construction at LLNL, with the goal of generating tunable γ-rays in the 0.5-2.5 MeV photon energy range, at a repetition rate of 120 Hz, and with a peak brightness in the 10^{20} photons/(s x mm^2 x mrad^2 x 0.1% bw).

* This work performed under the auspices of the U.S. DoE by LLNL under Contract DE-AC52-07NA27344 and by DHS DNDO.
#hartemann1@llnl.gov

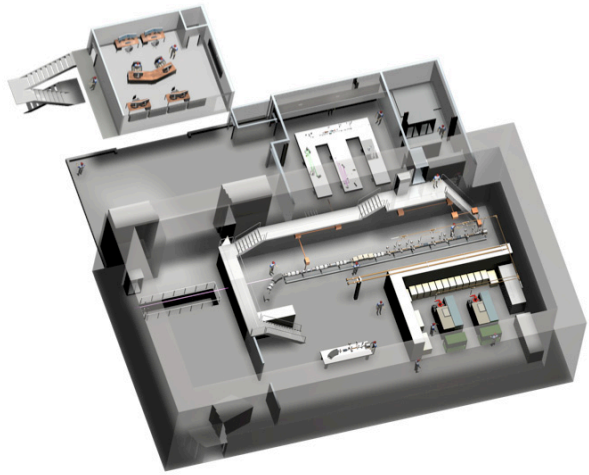

Figure 1: The MEGa-ray facility.

COMPTON SCATTERING

This section is a brief summary of the main properties of Compton scattering. The incident electron and photon 4-momenta are given by $u_\mu = (\gamma, \mathbf{u})$ and $k_\mu = (k, \mathbf{k})$; the scattered photon 4-wavenumber is $q_\mu = (q, \mathbf{q})$, and the electron 4-velocity after the interaction satisfies energy-momentum conservation: $v_\mu = u_\mu + \hbar(nk_\mu - q_\mu)$, where $\hbar$ is the reduced Compton wavelength and n is the harmonic (multi-photon) number. From these parameters, the incident and scattered light-cone variables can be computed [5], along with the Compton formula:

$$\frac{q}{k} = \frac{\gamma - u\cos(\varepsilon + \varphi)}{\gamma - u\cos\varepsilon + (1-\cos\varphi)\left\{\dfrac{\langle -A_\mu A^\mu \rangle}{2[\gamma - u\cos(\varepsilon+\varphi)]} + n\hbar k\right\}}.$$

Here, ε is the angle between the electron initial velocity and the mean electron beam axis; φ is the angle of incidence of the laser photon(s); $-A_\mu A^\mu$ corresponds to radiation pressure; finally, the result is given for on-axis radiation ($\theta = 0$). The relativistic Doppler upshift, radiation pressure, and recoil are the main contributions to

the scattered photon energy. This equation also shows that the frequency is very sensitive to both the electron beam and laser pulse phase spaces. Additional information can be derived from the Klein-Nishina differential scattering cross-section [4], 3D effects, and nonlinearities [5].

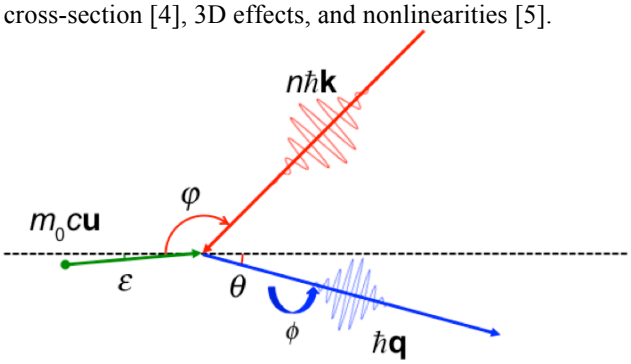

Figure 2: Interaction geometry.

X-BAND RF PHOTO-INJECTOR

The rf photoinjector is based on an earlier high gradient 7 MeV, 5.5-cell X-band rf photoinjector. Improvements specific to our application have been implemented and will be described in this paper. PARMELA simulations revealed that a longer first half- cell, as simulated with SUPERFISH resulted in a lower final emittance for the setup planned at LLNL. As a result a full redesign of the rf gun has been performed, using a longer first half-cell, lengthened from a 0.49 cell to a 0.59 cell. A schematic of the gun, low-energy beamline (LEB) and T53 is shown in Fig. 3.

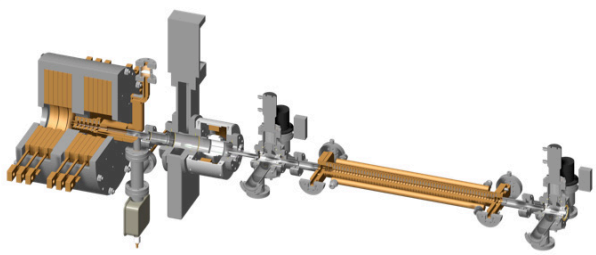

Figure 3: X-band rf gun, LEB, and T53 section.

Superior electron beam quality, with a normalized emittance of 0.4 mm.mrad at 250 pC charge, is ensured by the very high field applied to the photocathode: 200 MV/m, nominally. Full emittance compensation is implemented, with an optimum distance from the photocathode to the first accelerating section of 0.8 m.

The rf gun properties required for complete design are: field balanced across all cells, mode frequency of 11.424 GHz, and a coupling β of ~1.7. This new rf gun boasts an improved mode separation of >20 MHz, which decreases mode beating of the electric field on the cathode. The new rf gun also employs a racetrack coupler to reduce the rf quadrupole field experienced by the electron beam, and elliptically contoured irises to decrease the maximum surface electric field. These improvements were incorporated into the design of a modified rf gun for LLNL.

Complete 3D rf design for the photoinjector was accomplished using HFSS. Each modification affects the three design criteria: field balance is primarily a function of relative cell radii; coupling is primarily a function of the coupler cell radius and coupling aperture; the frequency is primarily changed by scaling all cell radii. Each adjustment changes the primary goal being modified, but also affects the other two. Final design is achieved by successive iteration, until all parameters are simultaneously met. The final field balance is quite excellent, and the final coupling was achieved at 11.424 GHz, with a β of ~1.7.

Final modification of the design is necessary to converge on a set of dimensions for engineering drawings and actual OFHC Cu fabrication. Machining will be done at 20ºC, while operation is planned for 45ºC. Scaling of the design dimensions was calculated and simulated. Design numbers were then truncated to acceptable fabrication tolerances, which required readjustment of the drawing numbers to conform with optimal field balance, coupling, and frequency at the operating temperature of 45ºC. Engineering drawings have been completed, and fabrication is planned in the near future.

0.5 GW X-BAND RF SYSTEM

The high power rf system is to provide adequate rf power to the accelerator to achieve the end-point electron energy. The accelerator consists of a X-band photo-gun and six sections of traveling wave accelerating structure, the T53VG3. The X-band photo-gun is a modified version of the 5.49 cells rf gun tested at SLAC in 2002. The rf budget for the gun is 20 MW and the fill time of the structure is 65 ns. The T53VG3 type travelling wave structure was extensively tested for high gradient operation and has operated at high gradient with low breakdown rates. The T-series structures are essentially the low group velocity (downstream) portion of the original 1.8 m structures. This structure can be operated with acceptable trip rate at gradients up to 90 MV/m. The fill time of this structure is 74.3 ns and an rf power of 70 MW is budgeted for each section.

The high power rf source is a X-band klystron (XL-4), which was developed by SLAC in the mid 90's for the high power testing of the X-band structures. The XL-4 is a solenoid focused klystron which requires a 0.47 Tesla solenoid. The high voltage pulse required by the klystron is provided by a state of the art, solid-state high voltage modulator. We have chosen the solid-state modulator (K2-3X) built by ScandiNova for its pulse-to-pulse stability and solid-state modular design; the first of these modulators has been delivered and is awaiting installation. Two klystrons and two high voltage modulators are planned for the LLNL MEGa-Ray project.

The high power pulsed rf output of two klystrons is 100 MW, 1.5 msec. The high power rf needs of the rf gun and accelerator sections are 440 MW for 210 ns (~ 3x fill time). The logical way to achieve this is to pulse compress the output of the klystrons to 500 MW, 210 ns and to

distribute the compressed pulse to the rf gun and accelerating sections. SLAC has developed and demonstrated SLED II with multi-mode delayed lines with similar power gain factor [8]. The dual-mode SLED-II delay lines will be approximately 15 meter long with inner diameter of 17 cm.

500 MW, 210 ns pulses are the desired output of the pulse compression system. These compressed pulses will be fed into a 13 dB coupler. The 13 dB (25MW) output will go to the rf gun. To allow for tuning and control, a phase shifter and attenuator are put in this arm. A barrier window is also planned for the rf gun. This is to limit the number of times the rf gun is exposed to air and to possibly provide for a configuration in which the rf gun can be baked and sealed as a unit before installation. The rest of the compressed power (475 MW) is to be distributed to the linear accelerator sections. A 3 dB H-hybrid is used to divide the 475 MW in half. Then a combination and 4.8 dB and 3 dB H-hybrids are used to distribute the power in one third portion (~ 70 MW) to each T53 section. Phase shifters and other control elements will be added as needed.

SYNCHRONIZATION

To ensure synchronization between the electron-generating laser pulse, the scattering laser pulse, and the electron-accelerating rf power, the fiber-based laser oscillator is used as a universal clock. The oscillator runs at a sub-harmonic of the rf design frequency (40.8 MHz for a 11.424 GHz accelerator), and provides seed light to both amplifier systems. The oscillator pulse train is monitored by a high-speed photodiode and the 11.424 GHz component of the signal is selected by a narrow band-pass filter, amplified, and delivered to the rf power system. Because the laser pulses start from the same oscillator, they are guaranteed to have good relative stability – all that is required it to match the travel time to the interaction point. Selecting correct pulses from the oscillator will get the pulses within 24 ns, and an extra length of optical fiber in the pre-amplification system can get to ~ns resolution. Final ps accuracy comes from an optical delay arm with micron accuracy.

PHOTOCATHODE DRIVE LASER

The photo-electrons are generated by a 50 μJ, 263 nm spatially and temporally shaped laser pulse. The oscillator seed is amplified (using standard chirped-pulse amplification [CPA] methods) in a series of Yb-doped fiber amplifiers, beginning with standard 6-μm core pre-amps, a 29 μm core intermediate photonic crystal fiber stage and a final 85 μm fiber rod amplifier to generate 1 mJ, 1053 nm pulses at 120 Hz that are compressed to 250 fs. These pulses are frequency quadrupled, stacked in a "Hyper-Michelson" pulse stacker, which converts the single input pulse into 8 replicas using 3 beam splitters; then transformed from Gaussian to a flat-top transverse profile using refractive optical beam shaping components. This beam is transported to the photoinjector, resized to 1 mm, and imaged onto the cathode surface.

INTERACTION LASER SYSTEM

Because the scattering laser should have minimal bandwidth and needs to be no shorter than 10 ps, Nd:YAG with its narrow gain bandwidth is a suitable material for amplification. Because of the narrow (< 1 nm) bandwidth and long (> ns) desired stretched pulse length in the amplification chain, we developed a novel hyper-dispersion stretcher and compressor pair [1] that provides very high (>7000 ps/nm) dispersion. The scattering laser pulse is generated by pre-amplifying a selected oscillator pulse in a 6 μm and 29 μm core fibers to the 30 μJ level, then doing final amplification in a set of diode-pumped Nd:YAG heads. The diode-pumping architecture allows this system to produce 1 J laser pulses at 120 Hz; subsequently compressed to 10 ps. This beam is then frequency-doubled to 532 nm and transported to the interaction region.

INTERACTION REGION

For the interaction of the laser and electron beams, a 180° geometry was chosen to maximize the gamma flux and minimize temporal tolerance. The electron beam is focused by a quadrupole triplet and re-collimated after the interaction by a matching triplet. The laser beam is focused by a 70 cm focal length lens, and steered onto the electron beam path by a dielectrically coated mirror with a hole in the center (which allows the electron beam to propagate through). The beam is collected by a similar mirror, on the other side of the interaction. To establish the relative alignment of the laser and electron beams, an optically polished nickel cube is located at the interaction point. Oriented with the vertical faces at 45° to the electron-laser beamline, the (significantly attenuated) laser reflects off the surface and the electron beam generates optical transition radiation light. These beams are imaged with a camera to ensure they are aligned vertically, and the overlap horizontally can be determined by seeing the beams meet at the edge. The light is also imaged onto a streak camera to allow the adjustment of the laser delay to get the correct temporal overlap.

REFERENCES

[1] M. Y. Shverdin, *et al*., Opt. Lett. **35**, 14 (2010).
[2] F. Albert, *et al*., Opt. Lett. **35**, 354 (2010).
[3] D.J. Gibson, *et al*., Phys. Rev. STAB **13**, 070703 (2010).
[4] F. Albert, *et al*., Phys. Rev. STAB **13**, 070704 (2010).
[5] L.M. Brown and R.P. Feynman, Phys. Rev. **85**, 231 (1952).
[6] G. Bhatt, *et al*., Phys. Rev. A **28**, 2195 (1983).
[7] F.V. Hartemann, *et al*., Phys. Rev. Lett., in press (2010).
[8] S. G. Tantawi, *et al*., Phy. Rev. STAB **8**, 042002 (2005).